Abstracta

Ano XIII - N. 01

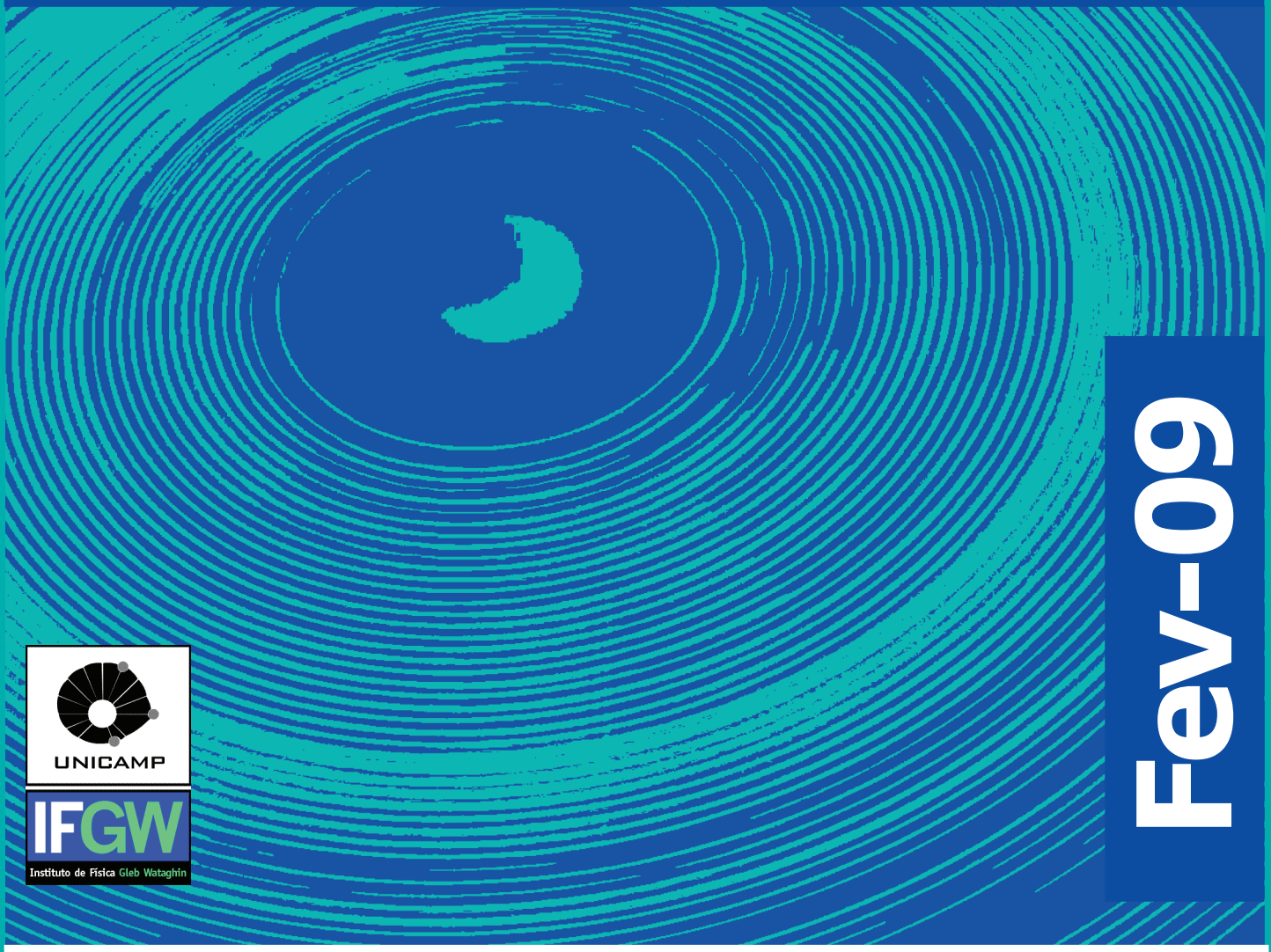

Fev-09

UNICAMP

IFGW

Instituto de Física Gleb Wataghin

Trabalhos Publicados

Dezembro 2008 à Fevereiro 2009

P001-09 à P048-09

Trabalhos Publicados

P001-09 "Accelerated Aging and Contact with Food Simulants in Adhesion of Amorphous Hydrogenated Carbon Films Obtained by the PECVD Process from Recycled PET from Packaging"

Cruz, S. A., Zanin, M., and de Moraes, M. A. B.

This work focuses principally on the influence of time, temperature, and contact with food simulants in adhesion of amorphous hydrogenated carbon (a-C:H) films obtained by the plasma enhanced chemical vapor deposition process in recycled PET from packaging. Shelf life of packaging used in soft drinks, fruit juice, etc. is known to be similar to 6 months, with possible variations. The a-C:H film, used in this study as a functional barrier against possible contaminants in recycled PET, was analyzed to determine possible alterations in its physical and chemical properties. The film underwent an accelerated aging test and was exposed to contact with food simulants listed by the FDA. In this case, adhesion is one of the properties most in need of conservation. This property was analyzed by means of the tape test and scanning electronic microscopy. Superficial chemical alterations resulting from both the accelerated aging test and contact with liquids were examined by the contact angle.

Journal of Applied Polymer Science 111[1], 281-290. 2009.

P002-09 "A comparative study of the magnetocaloric effect in RNi2 (R=Nd, Gd, Tb) intermetallic compounds"

Plaza, E. J. R., de Sousa, V. S. R., von Ranke, P. J., Gomes, A. M., Rocco, D. L., Leitao, J. V., and Reis, M. S.

Conventional and anisotropic magnetocaloric effects were studied in cubic rare earth RNi2 (R= Nd, Gd, Tb) ferromagnetic intermetallic compounds. These three compounds are representative of small, null, and large magnetocrystalline anisotropy in the series, respectively. Magnetic measurements were performed in polycrystalline samples in order to obtain the isothermal magnetocaloric data, which were confronted with theoretical results based on mean field calculations. For the R=Tb case, we explore the crystalline electrical-field anisotropy to predict the anisotropic magnetocaloric behavior due to the rotation of an applied magnetic field of constant intensity. Our results suggest the possibility of using both conventional and anisotropic magnetic entropy changes to extend the range of temperatures for use in the magnetocaloric effect.

Journal of Applied Physics 105[1]. 013903-013903-5. 2009.

P003-09 "A multi-screening approach for marine-derived fungal metabolites and the isolation of cyclodepsipeptides from Beauveria felina"

de Vita-Marques, A. M., Lira, S. P., Berlinck, R. G. S., Seleghim, M. H. R., Sponchiado, S. R. P., Tauk-Tornisielo, et all

Extracts obtained from 57 marine-derived fungal strains were analyzed by HPLC-PDA, TLC and H-1 NMR. The analyses showed that the growth conditions affected the chemical profile of crude extracts. Furthermore, the majority of fungal strains which produced either bioactive of chemically distinctive crude extracts have been isolated from sediments or marine algae. The chemical investigation of the antimycobacterial and cytotoxic crude extract obtained from two strains of the fungus Beauveria felina have yielded cyclodepsipeptides related to destruxins. The present approach constitutes a valuable tool for the selection of fungal strains that produce chemically interesting or biologically active secondary metabolites

Quimica Nova 31[5], 1099-1103. 2008.

P004-09 "Changes on White and Grey Matter Volume After Successful Surgery for Refractory Mtle Revealed by Voxel Based Morphometry (Vbm)"

Yasuda, C. L., Valise, C., Saude, A., Pereira, F., Costa, A., Morita, M., Betting, L. E., Castellano, G., Tedeschi, H., Oliveira, E., and Cendes, F. Journal

Epilepsia 49, 481-482. 2008.

P005-09 "Conductivity of electronic liquid-crystalline mesophases"

Fernandes, R. M., Schmalian, J., and Westfahl, H.

We investigate the connection between the transport properties and the thermodynamics of electronic systems with a tendency to form broken-symmetry mesophases evocative of the physics of liquid crystals. Through a hydrodynamic approach to the electronic transport in inhomogeneous systems, we develop a perturbative expansion for the macroscopic conductivity to study the transport of two-dimensional smectic and nematic phases. At the fluctuation-induced first-order phase transition expected for the smectic to isotropic transition, a jump in the macroscopic conductivity is predicted, with a directional dependence that reflects the fluctuation spectrum of the order parameter. When elastic fluctuation modes melt the smectic phase into a nematic phase, the resultant nematic order parameter is shown to be linearly proportional to the conductivity anisotropy. We also outline qualitative comparisons with recent experimental works on strongly correlated materials that show evidences of electronic liquid-crystalline mesophases

Physical Review B 78[18]. 184201. 2008.

P006-09 "Delocalization of vibrational normal modes in double chains: Application to DNA systems"

Paez, C. J. and Schulz, P. A.

In this work we investigate the localization of normal modes for several heuristic models of DNA like chains. The main finding is a possible robust normal mode delocalization in a finite low frequency range, irrespective of sequencing.

Microelectronics Journal 39[11], 1222-1223. 2008.

P007-09 "Dibucaine effects on structural and elastic properties of lipid bilayers"

Lorite, G. S., Nobre, T. M., Zaniquelli, M. E. D., de Paula, E., and Cotta, M. A.

In this work we report the interaction effects of the local anesthetic dibucaine (DBC) with lipid patches in model membranes by Atomic Force Microscopy (AFM). Supported lipid bilayers (egg phosphatidylcholine, EPC and dimyristoylphosphatidylcholine, DMPQ were prepared by fusion of unilamellar vesicles on mica and imaged in aqueous media. The AFM images show irregularly distributed and sized EPC patches on mica. On the other hand DMPC formation presents extensive bilayer regions on top of which multibilayer patches are formed. In the presence of DBC we observed a progressive disruption of these patches, but for DMPC bilayers this process occurred more slowly than for EPC. In both cases, phase images show the formation of small structures on the bilayer surface suggesting an effect on the elastic properties of the bilayers when DBC is present.

Dynamic surface tension and dilatational surface elasticity measurements of EPC and DMPC monolayers in the presence of DBC by the pendant drop technique were also performed, in order to elucidate these results. The curve of lipid monolayer elasticity versus DBC concentration, for both EPC and DMPC cases, shows a maximum for the surface elasticity modulus at the same concentration where we observed the disruption of the bilayer by AFM. Our results suggest that changes in the local curvature of the bilayer induced by DBC could explain the anesthetic action in membranes.

Biophysical Chemistry 139[2-3], 75-83. 2009.

P008-09 "Diffraction-enhanced imaging microradiography applied in breast samples"

Rocha, H. S., Pereira, G. R., Faria, P., Kellermann, G., Mazzaro, I., Tirao, G., Giles, C., and Lopes, R. T.

The diffraction-enhanced imaging (DEI) is a powerful tool to observe turners and other diseases in breast tissue and provide more precise diagnostics. In this work DEI was used to analyze breast tissues details that have poor attenuation contrast. An X-ray imaging system with DEI techniques was developed using synchrotron radiation. The DEI experiment was performed in D10A-XRD2 beamline at the Brazilian Synchrotron-LNLS. The pre-monochromator, upstream of the beamline was adjusted to 10.7 keV. The samples were positioned between two channel-cut Si(3 3 3) in non-dispersive geometry mounted in a double axes diffractometer. A direct conversion watercooled CCD camera of 1242 pixel x 1152 pixel of 25 mu m x 25 mu m each was used as a two-dimensional detector in scanning mode. The DEI system could show details in low attenuation tissues based on the contrast imaging obtained by attenuation, refraction gradient and ultra-small angle scatter characteristics. In this work the capacity to observe different types of Structures and details in breast tissues were investigated.

European Journal of Radiology 68[3], S37-S40. 2008.

P009-09 "Direct determination of the crystal field parameters of Dy, Er, and Yb impurities in the skutterudite compound CeFe4P12 by electron spin resonance"

Garcia, D. J., Garcia, F. A., Duque, J. G. S., Pagliuso, P. G., Rettori, C., Schlottmann, P., Torikachvili, M. S., and Oseroff, S. B.

Despite extensive research on the skutterudites for the last decade, their electric crystalline field ground state is still a matter of controversy. We show that electron spin resonance (ESR) measurements can determine the full set of crystal field parameters (CFPs) for the T-h cubic symmetry (Im3) of the Ce1-xRxFe4P12 (R=Dy, Er, Yb; x less than or similar to 0.003) skutterudite compounds. From the analysis of the ESR data the three CFPs B-4(c), B-6(c), and B-6(t) were determined for each of these rare earths at the Ce3+ site. The field and temperature dependence of the measured magnetization for the doped crystals is in excellent agreement with the one predicted by the CFPs B-n(m) derived from ESR

Physical Review B 78[17]. 174428. 2008.

P010-09 "Effect of Low Intensity Helium-Neon (HeNe) LaserIrradiation on Experimental Paracoccidioidomycotic Wound Healing Dynamics"

Ferreira, M. C., Gameiro, J., Nagib, P. R. A., Brito, V. N., Vasconcellos, E. D. C., and Verinaud, L.

The effect of HeNe laser on the extracellular matrix deposition,chemokine expression and angiogenesis in experimental paracoccidioidomycotic lesions was investigated. At days 7, 8 and 9 postinfection the wound of each animal was treated with a 632.8 nm HeNe laser at a dose of 3 J cm(-2). At day 10 postinfection, the wounds were examined by using histologic and immunohistochemical methods. Results revealed that lasertreated lesions were lesser extensive than untreated ones, and composed mainly by macrophages and lymphocytes. High IL-1 beta expression was shown in the untreated group whereas in laser-treated animals the expression was scarce. On the other hand, the expression of CXCL-10 was found to be reduced in untreated animals and quite intensive and well distributed in the laser-treated ones. Also, untreated lesions presented vascular endothelial growth factor (VEGF) in a small area near the center of the lesion and high immunoreactivity for hypoxia-inducible factor-1 (HIF-1), whereas laser-treated lesions expressed VEGF surrounding blood vessels and little immunoreactivity for HIF-1. Laser-treated lesions presented much more reticular fibers and collagen deposition when compared with the untreated lesion. Our results show that laser was efficient in minimizing the local effects observed in paracoccidioidomycosis and can be an efficient tool in the treatment of this infection, accelerating the healing process

Photochemistry and Photobiology 85[1], 227-233. 2009.

P011-09 "Effect of Therapeutic Dose X Rays on Mechanicaland Chemical Properties of Esthetic Dental Materials"

da Cruz, A. D., Sinhoreti, M. A. C., Ambrosano, G. M., Rastelli, A. N. D., Bagnato, V. S., and Boscolo, F. N.

The aim of this study was to investigate the influence of therapeutic dose X rays on the microhardness (MH) and degree of conversion (DC) of two different esthetic restorative dental materials. The materials were photo-activated with a LED lightcuring unit using three cure-times: 5, 20 and 40 seconds. The photo-activation was carried out in two distinct periods: before and after irradiation with doses of 5, 35 and 70 Gy, from a 6 MVX rays beam. In accordance with the methodology used, it was conclude that a therapeutic dose does not have a detrimental effect on the photoinitiator molecules, because the photo-activation occurred after they were irradiated. When the irradiation was applied before photo-activation, the materials showed MH improvement, but when photo-activation was performed after irradiation, there was less improvement. However, there was no correlation between MH and DC. Thus, a therapeutic dose applied to cured material can promote linking and breaking of chain bonds in a non-linear way Materials Research-Ibero-American

Journal of Materials 11[3], 313-318. 2008.

P012-09 "Effects of hydrostatic pressure on the Coulombbound states in GaAs-Ga1-xAlxAs semiconductor superlattices"

Vargas, J., Raigoza, N., Morales, A. L., Duque, C. A., and Reyes-Gomez, E.

The effects of hydrostatic pressure on the Coulomb-bound states in GaAs-Ga1-xAlxAs and GaAs-AlAs semiconductor superlattices are theoretically studied. Calculations of the impurity binding energies for different configurations of the system and for various values of the hydrostatic pressure are performed in the framework of the parabolic-band and effective-mass schemes, and within the variational procedure. The hydrostatic-pressure dependence on the exciton energy is also obtained, and theoretical results are compared and found in good agreement with available experimental measurements.

Superlattices and Microstructures 44[6], 809-813. 2008.

P013-09 "Effects of nitrogen ion irradiation on plasma polymerized films produced from titanium tetraiso pro poxide-oxygen-helium mixtures"

Da Cruz, N. C., Lopes, B. B., Rangel, E. C., de Moraes, M. A. B., and Durrant, S. F.

In this work films were produced by the plasma enhanced chemical vapor deposition (PECVD) of titanium tetraisopropoxide-oxygen-helium mixtures and irradiated with 150 keV singly-charged nitrogen ions (N+) at fluences, phi, between 10(14) and 10(16) cm(-2). Irradiation resulted in compaction, which reached about 40% (measured via the film thickness) at the highest fluence. Infrared reflection-absorption spectroscopy (IRRAS) revealed the presence of Ti-O bonds in all films. Both O-H and C-H groups were present in the asdeposited films, but the density of each of these decreased with increasing phi and was absent at high phi, indicating a loss of hydrogen. X-ray photoelectron spectroscopy (XPS) analyses revealed an increase in the C to Ti atomic ratio as phi increased, while the O to Ti ratio hardly altered, remaining at around 2.8. The optical gap of the films, derived from data obtained by ultraviolet-visible spectroscopy (UVS), remained at about 3.6 eV for all fluences except the highest, for which an abrupt fall to around 1.0 eV was observed. For the irradiated films, the electrical conductivity, measured using the two-point method, showed a systematic increase with increasing phi.

Surface & Coatings Technology 203[5-7], 534-537. 2008.

P014-09 "Electron Lande g(parallel to) factor in semiconductor quantum wires"

Lopez, F. E., Reyes-Gomez, E., and Oliveira, L. E.

The properties of the conduction-electron g(parallel to) factor in semiconductor GaAs-Ga1-xAlxAs quantum-well wires under magnetic fields applied along the wire axis are presented. The electron g(parallel to) factor is obtained as a function of both the applied magnetic field and transversal area of the wire. Calculations are performed by taking into account the nonparabolicity and anisotropy of the conduction band via the Ogg-McCombe Hamiltonian for both cylindrical and rectangular quantum-well wires. The conduction-electron Lande factor is shown to be a growing function of the applied magnetic field as well as dependent on the shape of the transversal section of the wire.

Microelectronics Journal 39[11], 1272-1273. 2008.

P015-09 "Evaluate the Waste Fatty Acid by Scientific and Technical Study to Obtain Biodiesel"

Barros, A. A. C., Wust, E., and Meier, H. F.

Waste fatty acid, from fatty boxes was evaluated as feedstock to obtain biodiesel in a laboratory scale. The residues were desemulsified, purified and used to obtain ethyl esters, through the transesterification with alkaline catalysis andesterification with acid catalysis reactions. The product was purified by adsorption in column of silica, and characterized by GLC with mass detector. Using this methodology the fatty residues was converted in the ethyl esters showed the scientific e technical validation of this propose. The conversion of fatty acids in ethylic esters was calculated by mass balances processes same for the highs degradation ofthe residue evaluates. To purify the biodiesel and glycerol obtained was necessary secondary processes to increase the qualities of this full and to use the glycerin in many industrial processes

Engenharia Sanitaria e Ambiental 13[3], 255-262. 2008.

P016-09 "Exploring neuro-vascular and neuro-metabolic coupling in rat somatosensory cortex"

Mesquita, R. C., Huppert, T. J., and Boas, D. A.

The existence of a coupling between changes in neuronal activity, cerebral blood flow and blood oxygenation is well known. The explicit relationship between these systems, however, is complex and remains a subject of intense research. Here, we use direct electrophysiological recordings to predict blood flow and oxygenation changes measured with optical methods during parametric stimulation applied to the somatosensory cortex in rat brain. Using a multimodal model of the cerebral functional unit, we estimate a neurovascular and a neuro-metabolic transfer function relating the experimentally measured neural responses with the inputs to a vascular model predicting hemodynamic and blood oxygenation changes. We show that our model can accurately predict experimentally measured parametric hemodynamic evoked responses by using a single linear transfer function relationship with a reduced number of state parameters to relate the level of neural activity to evoked cerebral blood flow and oxygen metabolism changes. At the same time, we characterize the metabolic and vascular neural response functions and interpret their physiological significance

Physics in Medicine and Biology 54[2], 175-185. 2009.

P017-09 "Field-trial evaluation of the Q-factor penalty introduced by fiber four-wave mixing wavelength converters"

Marconi, J. D., Callegari, F. A., Abbade, M. L. F., and Fragnito, H. L.

The performance of tunable all-optical wavelength converters based on four-wave mixing in optical fibers is experimentally tested in a field-trial network. Two converters were built with two different fibers. The first one was made with a small variation in the zero-dispersion wavelength (ZDW) dispersion shifted fiber and the second one with a highly nonlinear fiber that presents great ZDW variations. In order to compare the tuning ranges obtained in both cases we present an experimental spectral analysis. Numerical simulations that consider the influence of both the dispersion slope and the long-scale ZDW variations of the fiber complement the experiments. The tuning bandwidth was larger in the highly nonlinear fiber case. For a set of different optical signal-to-noise ratios, the measurements of the Q-factor of the signal and those of the converted wave are our main results. These results show that the penalty imposed by the converters is different for each converted wavelength. The maximum penalty obtained for the Q-factor was similar to 6 dB, but it was <= 3 dB for most cases. In all experiments we used a technique based on a dynamic polarization controller in order to avoid power fluctuations in the converted wave caused by polarization induced variations in the signal.

Optics Communications 282[1], 106-116. 2008.

P018-09 "Forward Neutral-Pion Transverse Single-Spin Asymmetries in p plus p Collisions at s=200 GeV"

Abelev, B. I., Aggarwal, M. M., Ahammed, Z., Anderson, B. D., Arkhipkin, D., Averichev, G. S.et all

We report precision measurements of the Feynman x (x(F)) dependence, and first measurements of the transverse momentum (p(T)) dependence, of transverse single-spin asymmetries for the production of pi(0) mesons from polarized proton collisions at s=200 GeV. The x(F) dependence of the results is in fair agreement with perturbative QCD model calculations that identify orbital motion of quarks and gluons within the proton as the origin of the spin effects. Results for the p(T) dependence at fixed x(F) are not consistent with these same perturbative QCD-based calculations

Physical Review Letters 101[22]. 222001. 2008.

P019-09 "gamma-Fe2O3 nanoparticles dispersed in porous Vycor glass: A magnetically diluted integrated system"

Cangussu, D., Nunes, W. C., Correa, H. L. D., Macedo, W. A. D., Knobel, M., Alves, O. L., Souza, A. G., and Mazali, I. O.

An investigation of the effect of interparticle interaction and particle size distribution has been carried out on iron oxide nanoparticles dispersed into porous Vycor glass. gamma-Fe2O3 nanoparticles dispersed into monoliths of Vycor glass were obtained using impregnation-decomposition cycles through the single-source metallo-organic decomposition process. Magnetic properties were investigated by ac magnetic susceptibility measurements, as a function of temperature at different frequencies, by measuring zero-field-cooled and field-cooled magnetization curves and by constructing hysteresis loops at different temperatures. A log-normal size distribution of monodomain nanoparticles has been deduced from the analysis of the magnetization curves. Fe-57 Mossbauer spectroscopy was also employed for investigating the magnetic behavior as a function of nanoparticle size. The systems exhibit typical superparamagnetic behaviors with a wide particle size distribution that can be changed without significantly affecting the interparticle interaction. The experimental data are discussed in terms of the evolution of the particle size distribution with the number of impregnation-decomposition cycles used for preparing the nanoparticles.

Journal of Applied Physics 105[1]. 013901-013901-7. 2009.

P020-09 "Generation of An Epr Pair of Atoms in Coupled Cavities System Via An Optical Fiber"

Yabu-Uti, B. F. C., Nohama, F. K., and Roversi, J. A.

The interaction between identical two-level atoms with a system that consists of two coupled cavities connected by an optical fiber was investigated. With new bosonic operators, the interaction Hamiltonian between the fiber and the cavities can be diagonalized (Pellizzari's model(1)). In the strong coupling regime (cavity field-fiber), the interaction between atoms and the non-resonant normal modes can be eliminated, simplifying our system to that of one atom interacting with a single-mode cavity. For this interaction, we have analyzed the entanglement between distant atoms. We present two simple procedures to generate two atoms in a maximally entangled state, interacting (i) successively and (ii) simultaneously with the coupled cavities system

International Journal of Quantum Information 6[5], 1021-1031. 2008.

P021-09 "Gravitational wave recoil in Robinson-Trautman spacetimes"

Macedo, R. P. and Saa, A.

We consider the gravitational recoil due to nonreflection-symmetric gravitational wave emission in the context of axisymmetric Robinson-Trautman spacetimes. We show that regular initial data evolve generically into a final configuration corresponding to a Schwarzschild black hole moving with constant speed. For the case of (reflection-)symmetric initial configurations, the mass of the remnant black hole and the total energy radiated away are completely determined by the initial data, allowing us to obtain analytical expressions for some recent numerical results that have appeared in the literature. Moreover, by using the Galerkin spectral method to analyze the nonlinear regime of the Robinson-Trautman equations, we show that the recoil velocity can be estimated with good accuracy from some asymmetry measures (namely the first odd moments) of the initial data. The extension for the nonaxisymmetric case and the implications of our results for realistic situations involving head-on collision of two black holes are also discussed

Physical Review D 78[10]. 104025. 2008.

P022-09 "Human FEZ1 has characteristics of a natively unfolded protein and dimerizes in solution"

Lanza, D. C. F., Silva, J. C., Assmann, E. M., Quaresma, A. J. C., Bressan, G. C., Torriani, I. L., and Kobarg, J.

The fasciculation and elongation protein Zeta 1 (FEZ1) is the mammalian orthologue of the Caenorhabditis elegans protein UNC-76, which is necessary for axon growth. Human FEZ1 interacts with Protein Kinase C (PKC) and several regulatory proteins involved in functions ranging from microtubule associated transport to transcriptional regulation. Theoretical prediction, circular dichroism, fluorescence spectroscopy, and limited proteolysis of recombinant FEZ1 suggest that it contains disordered regions, especially in its N-terminal region, and that it may belong to the group of natively unfolded proteins. Small angle X-ray scattering experiments indicated a mainly disordered conformation, proved that FEZ1 is a dimer of elongated shape and provided overall dimensional parameters for the protein. In vitro pull down experiments confirmed these results and demonstrated that dimerization involves the N-terminus. Ab-initio 3D low resolution models of the full-length conformation of the dimeric constructs 6xHis-FEZ1(1-392) and 6xHis-FEZ1(1-227) were obtained. Furthermore, we performed in vitro phosphorylation assays of FEZ1 with PKC. The phosphorylation occur-red mainly in its C-terminal region, and does not cause any significant conformational changes, but nonetheless inhibited its interaction with the FEZ1 interacting domain of the protein CLASP2 in vitro. The C terminus of FEZ1 has been reported to bind to several interacting proteins. This suggests that FEZ1 binding and transport function of interacting proteins may be subject to regulation by phosphorylation

Proteins-Structure Function and Bioinformatics 74[1], 104-121. 2009.

P023-09 "Interplay between coarsening and nucleation in an Ising model with dipolar interactions"

Cannas, S. A., Michelon, M. F., Stariolo, D. A., and Tamarit, F. A.

We study the dynamical behavior of a square lattice Ising model with exchange and dipolar interactions by means of Monte Carlo simulations. After a sudden quench to low temperatures, we find that the system may undergo a coarsening process where stripe phases with different orientations compete, or alternatively it can relax initially to a metastable nematic phase and then decay to the equilibrium stripe phase through nucleation. We measure the distribution of equilibration times for both processes and compute their relative probability of occurrence as a function of temperature and system size. This peculiar relaxation mechanism is due to the strong metastability of the nematic phase, which goes deep into the low-temperature stripe phase. We also measure quasiequilibrium autocorrelations in a wide range of temperatures. They show a distinct decay to a plateau that we identify as due to a finite fraction of frozen spins in the nematic phase. We find indications that the plateau is a finite-size effect. Relaxation times as a function of temperature in the metastable region show super-Arrhenius behavior, suggesting a possible glassy behavior of the system at low temperatures

Physical Review e 78[5]. 051602. 2008.

P024-09 "Intrinsic flavor violation for massive neutrinos"

Nishi, C. C.

It is shown that intrinsic neutrino flavor violation invariably occurs when neutrinos are created within the standard model augmented by the known massive neutrinos, with mixing and nondegenerate masses. The effects are very small but much greater than the naive estimate Delta m(2)/E nu(2) or the branching ratio of indirect flavor violating processes such as mu -> e gamma within the SM. We specifically calculate the probability (branching ratio) of pion decay processes with flavor violation, such as pi -> mu(nu) over bar (e), showing nonzero results

Physical Review D 78[11]. 113007. 2008.

P025-09 "Irreversibility in cooling and heating processes in the magnetocaloric MnAs and alloys"

Sharma, A. L. L., Gama, S., Coelho, A. A., and de Campos, A.

Irreversibility of adiabatic processes in the magnetocaloric MnAs and alloys is presented here. We used a differential scanning calorimeter to record the heat flux as a function of the temperature and applied field for MnAs (Mn,X)As, where X stands for Fe or Cu in 0.6% of doping. We extracted the latent heat and entropy in a cycle. In the cooling process, we observed that S-Mn(c)>S-Fe(c)>S-Cu(c), and for the heating process, S-Fe(h) approximate to S-Mn(h)>S-Cu(h). The difference in the entropy obtained between processes was found to be as high as 37%

Applied Physics Letters 93[26]. 261910. 2008.

P026-09 "Magnetic phase evolution in the LaMn(1-x)FexO(3+y) system"

de Lima, O. F., Coaquira, J. A. H., de Almeida, R. L., de Carvalho, L. B., and Malik, S. K.

We have investigated the crystal structure and magnetic properties for polycrystalline samples of LaMn1-xFexO3+y, in the whole range 0.0 <= x <= 1.0, prepared by solid state reaction in air. All samples show the ORT-2 orthorhombic structure that suppresses the Jahn-Teller distortion, thus favoring a ferromagnetic (FM) superexchange interaction between Mn3+-O-Mn3+. For x = 0.0 the oxygen excess (y approximate to 0.09) produces vacancies in the La and Mn sites and generates a fraction around 18% of Mn4+ ions and 82% of the usual Mn3+ ions, with possible double-exchange interaction between them. The Fe doping in this system is known to produce only stable Fe3+ ions. We find an evolution from a fairly strong FM phase with a Curie temperature T-C similar to 160 K, for x = 0.0, to an antiferromagnetic (AFM) phase with T-N = 790 K, for x = 1.0, accompanied by clear signatures of a cluster-glass behavior. For intermediate Fe contents a mixed-phase state occurs, with a gradual decrease (increase) in the FM (AFM) phase, accompanied by a systematic transition broadening for 0.2 < x < 0.7. A model based on the expected exchange interaction among the various magnetic-ion types accounts very well for the saturation magnetization (M-S) dependence on Fe doping.

Journal of Applied Physics 105[1]. 907-909. 2009.

P027-09 "Magnetocaloric effect: Overcoming the magnetic limit"

Plaza, E. J. R. and Campoy, J. C. P.

We have studied anomalous peaks observed in magnetocaloric -Delta S(T) curves for systems that undergo first-order magnetostructural transitions. The origin of those peaks, which can exceed the conventional magnetic limit, Rln(2J+1), is discussed on thermodynamic bases by introducing an additional-exchange contribution (due to exchange constant variation arising from magnetostructural transition). We also applied a semiphenomenological model to include this additional-exchange contribution in Gd5Si2Ge2 and MnAs-based systems, obtaining excellent results for the observed magnetocaloric effect.

Journal of Magnetism and Magnetic Materials 321[5], 446-449. 2008.

P028-09 "Metabolic Profiling of Pediatric Brain Tumors by Hrmas"

Cuellar, S., Morales, J., Calvar, J., Martinetto, H., Celda, B., Cerda-Nicolas, M., and Monleon, D.

Neuro-Oncology 10[6], 1102-1103. 2008.

P029-09 "New highly fluorescent biolabels based on II-VI semiconductor hybrid organic-inorganic nanostructures for bioimaging"

Santos, B. S., Farias, P. M. A., Menezes, F. D., Brasil, A. G., Fontes, A., Romao, L., Amaral, J. O., Moura-Neto, V., Tenorio, D. P. L. A., Cesar, C. L., Barbosa, L. C., and Ferreira, R.

Semiconductor quantum dots based on II - VI materials may be prepared to develop good biolabeling properties. In this study we present some well-succeeded results related to the preparation, functionalization and bioconjugation of CdY (Y=S, Se and Te) to biological systems (live cells and fixed tissues). These nanostructured materials were prepared using colloidal synthesis in aqueous media resulting nanoparticles with very good optical properties and an excellent resistance to photodegradation.

Applied Surface Science 255[3], 790-792. 2008.

P030-09 "Non-Markovian damping of Rabi oscillations in semiconductor quantum dots"

Mogilevtsev, D., Nisovtsev, A. P., Kilin, S., Cavalcanti, S. B., Brandi, H. S., and Oliveira, L. E.

A systematic investigation is performed on the damping of Rabi oscillations induced by an external electromagnetic field interacting with a two-level semiconductor system. We have considered a coherently driven two-level system coupled to a dephasing reservoir and shown that, to explain the dependence of the dephasing rate on the driving intensity, it is essential to consider the non-Markovian character of the reservoir. Moreover, we have demonstrated that intensity-dependent damping may be induced by various dephasing mechanisms due to stationary as well as non-stationary effects caused by coupling with the environment. Finally, present results are able to explain a variety of experimental measurements available in the literature

Journal of Physics-Condensed Matter 21[5]. 055801. 2009.

P031-09 "Non-parabolicity and anisotropy effects on the conduction-electron effective g factor in GaAs-Ga1-xAlxAs quantum well wires"

Lopez, F. E., Reyes-Gomez, E., and Oliveira, L. E.

The effective electron Lande factor in GaAs-Ga1-xAlxAs rectangular quantum well wires, under magnetic fields applied along the wire axis, is studied by taking into account the non-parabolicity and anisotropy of the conduction band within the Ogg-McCombe effective Hamiltonian. Confinement effects on the electron wavefunctions are explored in order to evaluate its influence on the behavior of the effective Lande factor. Calculations for the electron g(parallel to) factor in GaAs-Ga1-xAlxAs rectangular quantum well wires are compared with the previous theoretical results obtained for GaAs-Ga1-xAlxAs cylindrical quantum well wires. Such comparison clearly indicates the influence of the wire shape on the electron Lande factor in GaAs-Ga1-xAlxAs quantum well wires.

Physica E-Low-Dimensional Systems & Nanostructures 41[2], 240-244. 2008.

P032-09 "Numerical simulation of small angle scattering (SAXS) for large atomic clusters"

de Castro, A. R. B., Eremina, E., Bostedt, C., Hoener, M., Thomas, H., and Moller, T.

In the context of direct imaging of single nanoparticles, we discuss strategies for simulation of the small angle X-ray scattering (SAXS) of nanoparticles, propose a new scalar numerical approach applicable to arbitrary collections of atoms and compare it to the existing alternatives, both scalar and vector. The simulations are also compared with SAXS experimental data obtained recently at the FLASH FEL in Hamburg (lambda(FEL) 32 nm), demonstrating the direct evaluation of size for very large Argon clusters with a single FEL pulse.

Journal of Electron Spectroscopy and Related Phenomena 166, 21-27. 2008.

P033-09 "Radial current density effects on rotating magnetic field current drive in field-reversed configurations"

Clemente, R. A., Gilli, M., and Farengo, R.

Steady state solutions, suitable for field-reversed configurations (FRCs) sustained by rotating magnetic fields (RMFs) are obtained by properly including three-dimensional effects, in the limit of large FRC elongation, and the radial component of Ohm's law. The steady electrostatic potential, necessary to satisfy Ohm's law, is considered to be a surface function. The problem is analyzed at the midplane of the configuration and it is reduced to the solution of two coupled nonlinear differential equations for the real and imaginary parts of the phasor associated to the longitudinal component of the vector potential. Additional constraints are obtained by requesting that the steady radial current density and poloidal magnetic flux vanish at the plasma boundary which is set at the time-averaged separatrix. The results are presented in terms of the degree of synchronism of the electrons with the RMF and compared with those obtained when radial current effects are neglected. Three important differences are observed when compared with the case without radial current density. First, at low penetration of the RMF into the plasma there is a significant increase in the driven azimuthal current. Second, the RMF amplitude necessary to access the high synchronism regime, starting from low synchronism, is larger and the difference appears to increase as the separatrix to classical skin depth ratio increases. Third, the minimum RMF amplitude necessary to sustain almost full synchronism is reduced.

Physics of Plasmas 15[10]. 102503. 2008.

P034-09 "Scrutinizing localization properties in heuristic models for DNA molecules: Localization lengths versus participation ratios"

Carrillo-Nunez, H. and Schulz, P. A.

In this work we analyze the localization of electronic states of low-dimensional systems. We choose a well known strictly one-dimensional chain and an heuristic model for DNA-like molecules in order to compare two established methods for analyzing the degree of localization, namely the localization length and participation ratio.

Microelectronics Journal 39[11], 1220-1221. 2008.

P035-09 "Search for Active Neutrino Disappearance Using Neutral-Current Interactions in the MINOS Long-Baseline Experiment"

Adamson, P., Andreopoulos, C., Arms, K. E., Escobar, C. O., etc all

We report the first detailed comparisons of the rates and spectra of neutral-current neutrino interactions at two widely separated locations. A depletion in the rate at the far site would indicate mixing between nu(mu) and a sterile particle. No anomalous depletion in the reconstructed energy spectrum is observed. Assuming oscillations occur at a single mass-squared splitting, a fit to the neutral- and charged-current energy spectra limits the fraction of nu(mu) oscillating to a sterile neutrino to be below 0.68 at 90% confidence level. A less stringent limit due to a possible contribution to the measured neutral-current event rate at the far site from nu(e) appearance at the current experimental limit is also presented

Physical Review Letters 101[22]. 221804. 2008.

P036-09 "Structural and magnetic properties of nanocrystalline particles in an amorphous Fe73.5Nb3CuSi13.5B9 matrix"

Valenzuela, L. A., Duque, J. G. S., Meneses, C. T., Nunes, W. C., and Knobel, M.

We report structural and magnetic properties of fine particles embedded in an amorphous magnetic matrix. As-quenched amorphous Fe73.5Nb3CuSi13.5B9 ribbons (FINEMET) were submitted to the thermal treatments of several times (1 <= t <= 240 min) at 570 degrees C using a conventional furnace. The analyses of the X-ray diffraction patterns at room temperature reveal that our samples consist of single phase Fe3Si nanocrystals embedded in a residual amorphous phase. Magnetic measurements show that the saturation moment at T = 450 degrees C increases as a function of annealing time. This behavior is attributed to an increase of the fraction of nanocrystallites in the residual amorphous phase.

Journal of Non-Crystalline Solids 354[42-44], 4871-4873. 2008.

P037-09 "Structure determination of three-dimensional hafnium silicide nano structures on Si(100) by means of X-ray photoelectron diffraction"

Fluchter, C. R., de Siervo, A., Weier, D., Shurmann, M., Beimborn, A., Dreiner, S., Carazzolle, M. F., Landers, R., Kleiman, G. G., and Westphal, C.

We propose a modified zirconium silicide model for the structure of HfSi2 islands on Si(100). We studied this system in a combined investigation by means of photoelectron diffraction (XPD), photoelectron spectroscopy and atomic force microscopy. Synchrotron radiation was used for enhanced energy resolution and Surface sensitivity. Calculated XPD patterns of model clusters reflecting the structure as well as the morphology of the islands exhibit an excellent agreement with the experimental results.

From LEED and AFM measurements a preferential nano structure growth along the [011] and [0 (1) over bar1] direction was observed. Complementary XPD results clearly show that the HfSi2 structures are silicon terminated.

Surface Science 602[24], 3647-3653. 2008.

P038-09 "Studies of Fe-Cu microwires with nanogranular structure"

Zhukov, A., Garcia, C., Del Val, J. J., Gonzalez, J., Knobel, M., Serantes, D., Baldomir, D., and Zhukova, V.

We report on the fabrication, and structural and magnetic characterization of Cu63Fe37 microwires with granular structure produced by rapid quenching, using the TailorUlitovsky method, from the immiscible alloys. X-ray diffraction study demonstrated that the structure consists of small (6-45 nm) crystallites of Cu and body centred cubic alpha-Fe. Magnetic properties have been measured in the range of 5-300 K using a SQUID (superconducting quantum interference device) magnetometer. The temperature dependences of the magnetization measured in a cooling regime when no external magnetic field is applied (zero-field cooling) and in the presence of the field (field cooling) show considerable difference below 20 K. This difference could be related to the presence of small alpha-Fe grains embedded in the Cu matrix. Those alpha-Fe grains appear to be blocked at temperatures below that at which the maximum of the magnetization is observed in the low temperature range. Significant magnetoresistance (about 7%) has been found in the samples studied. The shape of the observed dependences is typical of a giant magnetoresistance effect

Journal of Physics-Condensed Matter 21[3]. 035301. 2009.

P039-09 "Study of nonlinear phenomena in four-component dusty plasma with charge fluctuation"

Sakanaka, P. H. and Spassovska, I.

The presence of a small quantity of positive dust component in a negatively charged dusty plasma gives rise to the double layers (DLs), which otherwise are absent. The parametric regions of solitons and DLs are given so as to guide experimenters to find this higher order nonlinear phenomenon experimentally. We also considered the case with the negative charge fluctuation so as to find in which conditions the charging equilibrium is reached and what is the consequence of the presence of the charge fluctuation on the linear dispersion relation

Physica Scripta T131. 014040. 2008

P040-09 "Synthesis and characterization of TM-doped CuO (TM = Fe, Ni)"

Meneses, C. T., Duque, J. G. S., Vivas, L. G., and Knobel, M.

Polycrystalline Cu1-xTMxO samples (x = 0 and 0.06; TM = Ni2+ and Fe3+) were grown using a co-precipitation method. The structural and magnetic properties were investigated by means of temperature dependent magnetic susceptibility and room temperature X-ray powder diffraction (XRPD). The XRPD analyses of the samples reveal the formation of single phase with structure isomorphous to the CuO. Interestingly, T-dependent magnetization shows the reduction of Neel temperature, T-N, from 213 K in the copper oxide to 70 K in the Fe-doped sample (x = 0.06). Because in the Ni-doped samples TN seems to be unaffected, this decrease in TN is believed to be due to the different electronic structure of the dopant. The ferromagnetic behavior observed at room temperature in all samples can be related to both the level of oxygen (excess or vacancy) of our samples and to the difference in the magnetic structure of the dopant.

Journal of Non-Crystalline Solids 354[42-44], 4830-4832. 2008.

P041-09 "Synthesis, structure and vibrational properties of GdIG(X):YIG(1-X) ferrimagnetic ceramic composite"

Fechine, P. B. A., Silva, E. N., de Menezes, A. S., Derov, J., Stewart, J. W., Drehman, A. J., Vasconcelos, I. F., Ayala, A. P., Cardoso, L. P., and Sombra, A. S. B.

Y3Fe5O12 (YIG) crystal has many attractive characteristics, such as low dielectric loss, narrow resonance linewidth in microwave region and also possesses a good saturated magnetization value. Composite technology in general sets out to combine materials in such a way that the properties of the composite are the optimum for a particular application. The different materials work together to give a composite of unique properties. In this work, we present the preparation procedure (obtaining) of the GdIG(x):YIG(1-X) ferrimagnetic ceramic matrix composite by mechanical alloying and calcinations. Besides that, we study its properties by X-ray powder diffraction, infrared, Micro-Raman, Fe-57 Mossbauer spectroscopy and hysteresis loop measurements.

Journal of Physics and Chemistry of Solids 70[1], 202-209. 2009.

P042-09 "System-Size Independence of Directed Flow Measured at the BNL Relativistic Heavy-Ion Collider"

Abelev, B. I., Aggarwal, M. M., Ahammed, Z., Anderson, B. D., Arkhipkin, D., Averichev, G. S., Bai, Y., Balewski, J., et all

We measure directed flow (v(1)) for charged particles in Au + Au and Cu + Cu collisions at root s(NN) = 200 and 62.4 GeV, as a function of pseudorapidity (eta), transverse momentum (p(t)), and collision centrality, based on data from the STAR experiment. We find that the directed flow depends on the incident energy but, contrary to all available model implementations, not on the size of the colliding system at a given centrality. We extend the validity of the limiting fragmentation concept to v(1) in different collision systems, and investigate possible explanations for the observed sign change in v(1)(p(t))

Physical Review Letters 101[25]. 252301. 2008.

P043-09 "Temperature dependence of molecular dynamics and supramolecular aggregation in MEH-PPV films: A solid-state NMR, X-ray and fluorescence spectroscopy study"

Souza, A. A., Cossiello, R. F., Plivelic, T. S., Mantovani, G. L., Faria, G. C., Atvars, T. D. Z., Torriani, I. L., Bonagamba, T. J., and Deazevedo, E. R.

This article presents an investigation of the temperature induced modification in the microstructure and dynamics of poly[2-methoxy-5-(2'-ethylhexyloxy)-1,4-phenylenevinylene] (MEH-PPV) cast films using Wide-Angle X-ray Scattering (WAXS), solid-state Nuclear Magnetic Resonance (NMR), and Fluorescence Spectroscopy (PL). MEH-PPV chain motions were characterized as a function of temperature by NMR. The results indicated that the solvent used to cast the films influences the activation energy of the side-chain motions. This was concluded from the comparison of the activation energy of the toluene cast film, E-a = (54 +/- 8) kJ/mol, and chloroform cast film, E-a = (69 +/- 5) kJ/mol, and could be attributed to the higher side-chain packing provided by chloroform, that preferentially solvates the side chain in contrast to toluene that solvates mainly the backbone. Concerning the backbone mobility, it was observed that the torsional motions in the MEH-PPV have average amplitude of similar to 10 degrees at 300 K, which was found to be independent of the solvent used to cast the films. In order to correlate the molecular dynamics processes with the changes in the microstructure of the polymer, in situ WAXS experiments as a function of temperature were performed and revealed that the interchain spacing in the MEH-PPV molecular aggregates increases as a function of temperature,

particularly at temperatures where molecular relaxations occur. It was also observed that the WAXS peak associated with the bilayer spacing becomes narrower and its intensity increases whereas the peak associated with the inter-backbone planes reduces its intensity for higher temperatures. This last result Could be interpreted as a decrease in the number of aggregates and the reduction of the interchain species during the MEH-PPV relaxation processes. These WAXS results were correlated with PL spectra modifications observed upon temperature treatments.

European Polymer Journal 44[12], 4063-4073. 2008.

P044-09 "The giant anisotropic magnetocaloric effect in DyAl2"

von Ranke, P. J., de Oliveira, N. A., Plaza, E. J. R., de Sousa, V. S. R., Alho, B. P., Carvalho, A. M. G., Gama, S., and Reis, M. S.

We report on calculations of the anisotropic magnetocaloric effect in DyAl2 using a model Hamiltonian including crystalline electrical field effects. The anisotropic effect is produced by the rotation of a constant magnetic field from the easy to a hard magnetic direction in the crystal and is enhanced by the first order nature of the field induced spin reorientation transition. The calculated results indicate that for a field with modulus of 2 T rotating from a hard to the easy direction, the isothermal magnetic entropy (Delta S-iso) and adiabatic temperature (Delta T-ad) changes present peak values higher than 60% the ones observed in the usual process, in which the field direction is kept constant and the modulus of the field is varied.

Journal of Applied Physics 104[9]. 093906-093906-4. 2008.

P045-09 "The magnetized steel and scintillator calorimeters of the MINOS experiment"

Michael, D. G., Adamson, P., Alexopoulos, T., Escobar, C. O.,

The Main Injector Neutrino Oscillation Search (MINOS) experiment uses an accelerator-produced neutrino beam to perform precision measurements of the neutrino oscillation parameters in the "atmospheric neutrino" sector associated with muon neutrino disappearance. This long-baseline experiment measures neutrino interactions in Fermilab's NuMI neutrino beam with a near detector at Fermilab and again 735 km downstream with a far detector in the Soudan Underground Laboratory in northern Minnesota. The two detectors are magnetized steel-scintillator tracking calorimeters. They are designed to be as similar as possible in order to ensure that differences in detector response have minimal impact on the comparisons of event rates, energy spectra and topologies that are essential to MINOS measurements of oscillation parameters. The design, construction, calibration and performance of the far and near detectors are described in this paper.

Nuclear Instruments & Methods in Physics Research Section A-Accelerators Spectrometers Detectors and Associated Equipment 596[2], 190-228. 2008.

P046-09 "Three-dimensional quantitative structure-activity relationships for a large series of potent antitubercular agents"

Andrade, C. H., Salum, L. D., Pasqualoto, K. F. M., Ferreira, E. I., and Andricopulo, A. D.

Comparative molecular field analysis (CoMFA) studies were conducted on a series of 100 isoniazid derivatives as anti-tuberculosis agents using two receptor-independent structural data set alignment strategies: (1) rigid-body fit, and (2) pharmacophore-based. Significant cross-validated correlation coefficients were obtained (CoMFA(1), q(2) = 0,75 and CoMFA(2), q(2) = 0.74), indicating the potential of the models for untested compounds. The models were then used to predict the inhibitory potency of 20 test set compounds that were not included in the training set, and the predicted values were in good agreement with the experimental results

Letters in Drug Design & Discovery 5[6], 377-387. 2008.

P047-09 "Two-photon absorption spectrum in diazoaromatic compounds"

De Boni, L., Andrade, A. A., Yamaki, S. B., Misoguti, L., Zilio, S. C., Atvars, T. D. Z., and Mendonca, C. R.

This Letter studies the degenerate two-photon absorption (2PA) spectra of three diazoaromatic compounds using Z-scan with fs-pulses. The 2PA spectra exhibit resonant enhancement of the nonlinearity as the excitation approaches the linear absorption. The absence of 2PA to the pi pi* band is related to the weaker donor/acceptor groups, and lower symmetry of diazoaromatic compounds, in agreement with our semi-empirical calculations. The higher magnitude of the 2PA cross-section, in comparison with single azoaromatics, demonstrates the positive effect of increasing conjugation. The decrease of 2PA cross-section with temperature is attributed to thermally induced torsions, which decreases the effective conjugation of diazoaromatic molecules.

Chemical Physics Letters 463[4-6], 360-363. 2008.

P048-09 "Understanding the inverse magnetocaloric effect in antiferro- and ferrimagnetic arrangements"

von Ranke, P. J., de Oliveira, N. A., Alho, B. P., Plaza, E. J. R., de Sousa, V. S. R., Caron, L., and Reis, M. S.

The inverse magnetocaloric effect occurs when a magnetic material cools down under applied magnetic field in an adiabatic process. Although the existence of the inverse magnetocaloric effect was recently reported experimentally, a theoretical microscopic description is almost nonexistent. In this paper we theoretically describe the inverse magnetocaloric effect in antiferro- and ferrimagnetic systems. The inverse magnetocaloric effects were systematically investigated as a function of the model parameters. The influence of the Neel and the compensation temperature on the magnetocaloric effect is also analyzed using a microscopic model

Journal of Physics-Condensed Matter 21[5]. 056004. 2009.

Abstracta

Instituto de Física
Diretor: Prof. Dr. Júlio César Hadler Neto
Universidade Estadual de Campinas - UNICAMP
Cidade Universitária Zeferino Vaz
13083-859 - Campinas - SP - Brasil
e-mail: secdir@ifi.unicamp.br
Fone: 0XX 19 3521-5300

Publicação

Biblioteca do Instituto de Física Gleb Wataghin
http://webbif.ifi.unicamp.br
Diretora Técnica: Rita Aparecida Sponchiado

Elaboração
Antonela Carvalho Ribeiro
antonela@ifi.unicamp.br

Projeto Gráfico
ÍgneaDesign

Impressão

Gráfica Central - Unicamp